A Novel Method of Three-Dimensional Geometry Reconstruction of Space Targets Based on the ISAR Image Sequence

Zuobang Zhou[1], Rongzhen Du[1], Lei Liu[1], Feng Zhou[1*]
[1]*Key Laboratory of Electronic Information Countermeasure and Simulation Technology of Ministry of Education*
Xidian University
Xi'an, China
fzhou@mail.xidian.edu.cn

***Abstract*—Based on the inverse synthetic aperture radar image sequence of triaxial stabilized space targets, a novel method of three dimensional (3D) geometry reconstruction for space targets is proposed. We firstly construct the projection vectors connecting the 3D geometry and the 2D ISAR image sequence of a space target by utilizing ISAR imaging model and the radar line of sight (LOS). Then, by projecting the 3D scatterer candidates onto each imaging plane, we can accumulate the energy of the corresponding 2D scatterer in each image. The 3D scatterer candidates occupying larger accumulation energy are reserved as the real parts of the space target. Particle swarm optimization algorithm is applied to search the true 3D scatterers with high efficiency. The innovation of the proposed method lies in that it never needs the 2D scatterer extraction and association, which simplifies the reconstruction algorithm greatly compared with traditional 3D geometry reconstruction methods. Finally, experimental results based on the simulated point target are presented to validate the effectiveness and robustness of the proposed method.**

Keywords—Inverse synthetic aperture radar (ISAR), image sequence, projection vectors, 3D geometry reconstruction, particle swarm optimization (PSO)

I. INTRODUCTION

Inverse synthetic aperture radar (ISAR) can acquire two-dimensional (2D) high resolution images of space targets under all-day and all-weather conditions. Therefore, ISAR has been playing an important role in space targets observation and imaging[1]-[4]. However, a 2D ISAR image is only the projection of the 3D target geometry on the imaging plane. We cannot obtain further feature and structure information of the observed target from a 2D image. To achieve better recognition and classification performance, the 3D imaging method of the space target has become a hot research spot in the ISAR imaging field.

According to the number of the radar receiving channels, 3D ISAR imaging methods can be generally divided into two classes[5]: multi-channels-based 3D interferometric ISAR (In-ISAR) imaging methods [6]-[8] and single channel-based 3D ISAR imaging methods [9]-[15]. As for the first class, 3D geometry reconstruction of the observed target is achieved by making use of the interferometric phase terms, which are obtained from the interferometric processing of the 2D images of different receiving channels. In In-ISAR imaging, at least two receiving channels are needed to achieve the interferometric phase computation and height information estimation. Therefore, extra hardware design and signal processing algorithms must be considered. The second class of 3D imaging methods are based on the single receiving channel ISAR. Sequential 2D ISAR images are utilized to reconstruct the 3D geometry of the observed target[13]-[15]. Motivated by the factorization decomposition-based 3D geometry reconstruction methodology in optical image processing [11][12], 2D scatterers are extracted from the 2D ISAR image sequence and the scatterer trajectory matrix is estimated. By performing the factorization decomposition on the trajectory matrix, 3D geometry of the target can be reconstructed.

To obtain the 3D geometry of space targets, traditional factorization decomposition-based method can be applied. However, complex structure of space targets will lead to a huge decline in precision and efficiency of scatterer trajectory association. Therefore, a new reverse-projection-based 3D geometry reconstruction method is proposed. Since the attitude of triaxial stabilized space targets remain unchanged relative to the orbital coordinate system, we can derive the analytical relation between the 3D geometry and the projected positions of scatterers. Then, the energy distribution of sequential ISAR images can be projected reversely to the 3D space and the 3D positions of each scatterer will be obtained.

The remainder of this paper is presented as follows. Section II establishes the space target observation model and ISAR imaging model. The analytical relation between the 3D geometry of space targets and the 2D projected positions is also derived in this section. Section III presents the 3D geometry reconstruction method based on the ISAR image sequence. Section IV presents the experimental results based on the simulated data. Finally, the conclusion is drawn in Section V.

II. ISAR IMAGING AND SIGNAL MODEL

In ISAR imaging, the observed targets, such as aircrafts, missiles and ships, are generally uncooperative and the motion characteristics cannot be obtained in advance. However, the space targets must be moving in a specific orbit, which facilitates long-time and wide-angle ISAR observation. As for the normally working space targets, e.g. triaxial stabilized satellites, their attitudes will keep unchanged in the orbital coordinate system. The ISAR observation model is presented in Fig. 1 and O-XYZ is the

This paper was funded in part by the National Natural Science Foundation of China under Grant No. 61801344, No. 61801347 and No. 61631019; in part by the China Postdoctoral Science Foundation under Grant No. 2016M602775 and No. 2017M613076, in part by the Aeronautical Science Foundation of China under Grant 20181081003, in part by the Young Scientist Award of Shaanxi Province under Grant No. 2016YFXX-7 and in part by the Postdoctoral Science Research Projects of Shaanxi Province.

orbital coordinate system. O represents the target center and the OZ coordinate is toward from the target center to the earth center. The plane formulated by OZ coordinate and the moving direction of the space target is called the orbital plane. OX is located in the orbital plane and toward the moving direction. OY coordinate can be determined by the right hand rule. In Fig. 1, the green line represents the variation of the radar line of sight (LOS) while each red line is the instantaneous direction of the radar LOS. It can be seen that the radar LOS is not changing linearly. In order to better describe the variation, we denote the instantaneous azimuth angle and pitch angle as $\theta(t)$ and $\phi(t)$ where t is the observation time.

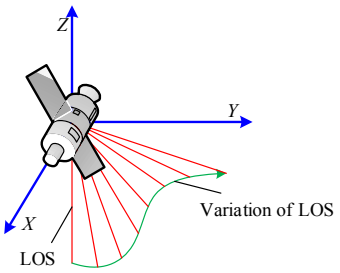

Fig. 1. Illustration of ISAR observation and imaging of a space target

As shown in Fig. 1, the variation of the radar LOS is non-stationary in the long time radar observation. Actually, the variation of the radar LOS can be considered as the non-stationary rotation of the space target. Therefore, the non-stationary ISAR echoes cannot be processed by traditional Range-Doppler (RD) imaging algorithm. To solve this problem, the long-time echoes of the space target are divided into overlapped sub-apertures and the detailed procedure can be found in [1]. The instantaneous radar LOS can be expressed as

$$\mathbf{l}=\left[-\cos\phi(t)\cos\theta(t),-\cos\phi(t)\sin\theta(t),-\sin\phi(t)\right]^T \tag{1}$$

If the instantaneous distance between the radar and the target center is denoted by $r_0(t)$, the instantaneous position of the radar will be

$$\mathbf{q}_t=\begin{bmatrix} r_0(t)\cos\phi(t)\cos\theta(t) \\ r_0(t)\cos\phi(t)\sin\theta(t) \\ r_0(t)\sin\phi(t) \end{bmatrix} \tag{2}$$

Since ISAR is generally far from the space target, the transmitted electromagnetic waves can be seen as the planar waves. Considering arbitrary scatterer $\mathbf{p}_n=[x_n,y_n,z_n]^T$, the projection of the distance from the radar to this scatterer on the radar LOS is

$$r(t)=(\mathbf{p}_n-\mathbf{q}_t)^T\times\mathbf{l} \tag{3}$$

By substituting $\mathbf{p}_n$, $\mathbf{p}_r$ and $\mathbf{l}$ in (3), and after translational motion component been compensated we can obtain the instantaneous distance of a specific scatterer to the radar

$$\begin{aligned} r_n(t)=&\Delta r_0-x_n\cos\phi(t)\cos\theta(t) \\ &-y_n\cos\phi(t)\sin\theta(t)-z_n\sin\phi(t) \end{aligned} \tag{4}$$

where Δr_0 represents the residual translational motion components. As is well known, the two dimensions of a 2D ISAR image are range dimension and cross-range dimension, respectively. The coordinate in range dimension denote the projection of the instantaneous distance between the scatterer and the radar on the radar LOS. The coordinate in cross-range dimension represent the Doppler of this scatterer. Actually, Doppler is proportional to the instantaneous velocity of the projection distance. Therefore, the cross-range coordinate of the scatterer can be expressed as

$$f_n=-\frac{2}{\lambda}\cdot\frac{\partial r_n(t)}{\partial t} \tag{5}$$

where λ denotes the transmitted electromagnetic signal wavelength. Combining (4) and (5), we can obtain

$$f_n=\frac{2}{\lambda}\left\{\begin{aligned} &x_n\left[-\frac{\partial\phi(t)}{\partial t}\cos\theta(t)\sin\phi(t)\right. \\ &\left.-\frac{\partial\theta(t)}{\partial t}\sin\theta(t)\cos\phi(t)\right] \\ &+y_n\left[-\frac{\partial\phi(t)}{\partial t}\sin\theta(t)\sin\phi(t)\right. \\ &\left.+\frac{\partial\theta(t)}{\partial t}\cos\theta(t)\cos\phi(t)\right] \\ &+z_n\frac{\partial\phi(t)}{\partial t}\cos\phi(t) \end{aligned}\right\} \tag{6}$$

Until now, we have obtained the instantaneous projection distance and the Doppler of arbitrary scatterer of the space target, which can be calculated directly from the images of different sub-aperture echoes. When dividing the long-time ISAR echoes, we can make the coherent integration time of each sub-aperture relative small. Therefore, the variation of the projection distance and the Doppler of the scatterers will be less than one range resolution cell and one cross-range resolution cell, respectively. Without losing generality, we can choose the projection distance and the Doppler of each scatterer in the intermediate time of each sub-aperture as the calculated positions from the corresponding image. Let

$$\omega_\theta(t)=\frac{\partial\theta(t)}{\partial t} \tag{7}$$

and

$$\omega_\phi(t)=\frac{\partial\phi(t)}{\partial t} \tag{8}$$

denote the angular velocities of the azimuth and pitch angles of the radar LOS, respectively. If the 2D position of the scatterer in each sub-aperture ISAR image is denoted by the instantaneous projection distance and the Doppler in the intermediate time of each sub-aperture, the projection equation of the 3D scatterer on the image plane of k -th sub-aperture can be expressed as

$$\begin{bmatrix} f_n^k \\ r_n^k \end{bmatrix}=\begin{bmatrix} \left(\boldsymbol{\rho}_a^k\right)^T \\ \left(\boldsymbol{\rho}_r^k\right)^T \end{bmatrix}\times\mathbf{p}_n \tag{9}$$

where n denotes the scatterer index of the space target.

$$\boldsymbol{\rho}_a^k=\frac{2}{\lambda}\begin{bmatrix} -\omega_\phi(t_k)\cos\theta(t_k)\sin\phi(t_k)-\omega_\theta(t_k)\sin\theta(t_k)\cos\phi(t_k) \\ -\omega_\phi(t_k)\sin\theta(t_k)\sin\phi(t_k)+\omega_\theta(t)\cos\theta(t_k)\cos\phi(t_k) \\ \omega_\phi(t_k)\cos\phi(t_k) \end{bmatrix} \tag{10}$$

denotes the projection vector of the 3D scatterer on the cross-range dimension.

$$\boldsymbol{\rho}_r^k=\left[-\cos\phi(t_k)\cos\theta(t_k),-\cos\phi(t_k)\sin\theta(t_k),-\sin\phi(t_k)\right]^T \tag{11}$$

denotes the projection vector of the 3D scatterer on the range dimension. In (10) and (11), t_k is the intermediate time of k -th sub-aperture. It can also be seen from (10) and (11) that $\boldsymbol{\rho}_r^k$ and $\boldsymbol{\rho}_a^k$ only depend on the direction and angular velocities of the radar LOS at t_k . Fortunately, the radar LOS sequence is known in space target observation and hence a sequence of projection equations can be formulated. Traditional ISAR image sequence-based 3D target geometry reconstruction methods need to associate the 2D scatterers extracted from the image sequence. The precise estimation of 2D scatterer trajectory matrix is a pre-requisite for the following factorization decomposition. However, the scatterer trajectory association algorithms must consider the anisotropy of the radar cross section and the occlusion of different scatterers, making the corresponding algorithms rather complex. To overcome this problem, we propose a new 3D geometry and structure reconstruction method by accumulating the energy distribution of ISAR image sequence. Since no scatterer extraction and trajectory association are needed, the proposed method is easier to implement.

III. Reverse Projection Based 3D Geometry Reconstruction

A. Generation of high resolution ISAR image sequence

As is discussed in the previous section, the long-time echoes should be divided into overlapped sub-apertures. The larger the coherent integrated interval of each sub-aperture is, the larger the relative rotational angle of the space target is, the higher the cross-range resolution of the corresponding sub-aperture image will be. However, large rotational angle may cause the migration through range cells (MTRC), making the final image defocused. Therefore, the Keystone transform can be applied to eliminate this phenomenon [16]. Lots of similar imaging algorithms [17]-[19] can be utilized to tackle the ISAR imaging problems under complex target motion and large rotational angle, which is not the focus of this paper. After the above processing, we can obtain the 2D high resolution ISAR image sequence of the space target.

B. Projection vectors construction

Through the imaging processing in the previous section, the high-resolution ISAR image sequence can be obtained. If we want to accumulate the scatterer energy of 2D image sequence, the projection vectors corresponding to the range and cross-range dimensions of each sub-aperture image should be constructed first. The space targets observation model is illustrated in Fig. 2, in which O-XYZ represents the orbital coordinate system and the direction of each axis has been clarified in Section 2. As for the triaxial stability satellites, their attitudes will keep unchanged relative to the O-XYZ coordinate system. O_2-UVW denotes the radar measurement coordinate system. Both O_2U coordinate and O_2V coordinate are parallel to the tangent plane of the radar relative to the earth surface. O_2U coordinate is toward the east while O_2V coordinate is toward the north. O_2W coordinate is determined by the right-hand rule. Since the radar position and the LOS sequence can be read from the radar measurement information, the directions of O_2-UVW coordinate system can be determined. If the transformation matrix between O_2-UVW coordinate system and O-XYZ coordinate system can be derived, the LOS vectors can be computed and expressed in the O-XYZ coordinate system. However, this transformation matrix is difficult to be obtained directly. To solve this problem, we transform the radar LOS vectors from the radar measurement coordinate (O_2-UVW) to the earth centered inertial coordinate system first, and then to the orbital coordinate system. If the radar LOS vector is denoted by $\mathbf{l}^{rd}$ in the radar measurement coordinate system, its expression in the orbital coordinate system can be expressed by

$$\mathbf{l}^{oc}=\mathbf{T}^1\times\mathbf{T}^2\times\mathbf{l}^{rd} \tag{12}$$

where $\mathbf{T}^1$ represents the transformation matrix from the earth centered inertial coordinate system to the orbital coordinate system, $\mathbf{T}^2$ denotes the transformation matrix from the radar measurement coordinate system to the earth centered inertial coordinate system. After obtaining $\mathbf{l}^{oc}$, we can compute the instantaneous azimuth angle $\theta(t)$ and elevation angle $\phi(t)$ of the radar LOS in the orbital coordinate system, as well as the azimuth angular velocity $\omega_\theta(t)$ and pitch angular velocity $\omega_\phi(t)$. Considering the first image frame as the initial observation time instant, we can construct the range projection vector $\boldsymbol{\rho}_r^k(1\le k\le K)$ and

the cross-range projection vector $\boldsymbol{\rho}_a^k (1 \le k \le K)$, which are corresponding to each image frame.

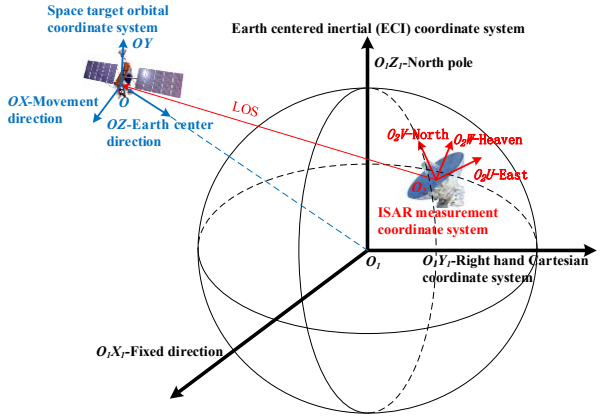

Fig. 2. Illustration of space targets observation model and corresponding coordinate systems

C. Reverse Projection

Through the division of wide-angle echoes and imaging processing of each sub-aperture, we can obtain high-resolution ISAR image sequence. Based on the radar measurement information of the space target, the projection vectors can be obtained. Considering a 3D scatterer candidate, we can compute its projection positions in each sub-aperture image. If this scatterer is from geometry the target, we can detect a peak energy in the image sequence. Actually, we must consider the anisotropy of the RCS and the occlusion of different scatterers and therefore the projected scatterer can be detected in part of the image sequence. However, if this scatterer candidate is not from geometry of the target, most of the projected positions in the image sequence would occupied by noise, whose energy will be lower than that of the true projected scatterer. Motivated by this fact, we can inversely project the energy distribution of 2D image sequence to the 3D space by accumulating the energy of the projected scatterer positions. Higher energy accumulation can be obtained from a real 3D scatterer candidate while lower energy accumulation will be acquired from a fake 3D scatterer candidate. The estimation of 3D scatterer candidate can be modeled as

$$\begin{aligned}\mathbf{p}_{opt} &= \arg\max_{\mathbf{p}} \sum_{k=1}^{K} \left[\mathbf{I}_k \left(\frac{\boldsymbol{\rho}_r^k \times \mathbf{p}}{\rho_r} + \frac{M_r}{2}, \frac{\boldsymbol{\rho}_a^k \times \mathbf{p}}{\Delta f_a} + \frac{M_a}{2} \right) \right] \\ &= \arg\max_{\mathbf{p}} \varpi\left(\mathbf{p} \,|\, \mathbf{I}_1, \mathbf{I}_2, \cdots, \mathbf{I}_K\right)\end{aligned} \quad (13)$$

where $\mathbf{p} = [x, y, z]^T$ denotes the 3D scatterer candidate, $\mathbf{I}_k$ is the k-th ISAR image. The range resolution cell and the cross-range resolution cell of $\mathbf{I}_k$ are ρ_r and Δf_a, respectively. Since the transmitted signal bandwidth and the pulse repetition frequency for each sub-aperture are the same, ρ_r and Δf_a are constants for all the image frames. M_r and M_a represent the sampling numbers of the range dimension and the cross-range dimension, respectively. The projected radial distance and Doppler of a 3D scatterer candidate are $\boldsymbol{\rho}_r^k \times \mathbf{p}$ and $\boldsymbol{\rho}_a^k \times \mathbf{p}$, respectively, which may not be integers. Therefore, interpolation processing will be applied to exactly compute the energy accumulation result for a given scatterer candidate. Equation (13) also shows that the 3D scatterer reconstruction of the space target can be modelled as an unconstrained optimization problem, whose cost function is $\varpi\left(\mathbf{p} \,|\, \mathbf{I}_1, \mathbf{I}_2, \cdots, \mathbf{I}_K\right)$. To solve this problem, the exhausted search is the easiest way available. However, huge computation burden is inevitable if small search step is set to achieve high estimation precision. Therefore, particle swarm optimization (PSO) is used here to search the 3D scatterer. Once a scatterer candidate is identified as a real one, the image pixels within a predetermined distance around the projected position of this identified scatterer would be set to zeros in each image frame. By the CLEAN processing, this identified scatterer will not be searched again. The detailed procedure is presented as follows.

Step 1) Initialization. Divide the ISAR compressed echoes into K sub-apertures and perform imaging algorithm on each sub-aperture to obtain the high resolution ISAR image sequence $\mathbf{I}_k (1 \le k \le K)$. According to the radar measurement information of the space target, we can compute the azimuth angle $\theta(t)$ and the pitch angle $\phi(t)$ of the radar LOS vector expressed in the orbital coordinate system. Then the projection vectors of the range dimension and the cross-range dimension are calculated as $\boldsymbol{\rho}_r^k (1 \le k \le K)$ and $\boldsymbol{\rho}_a^k (1 \le k \le K)$, respectively. Compute the total energy E_{total} of the ISAR image sequence and let $E_{remain} = E_{total}$. Initialize the upper bound of the scatterer number as $N_{\max}$. Calculate the ratio δ of the residual image energy and the initial total image energy. Initialize the 3D scatterer set as $\Theta = \varnothing$.

Step 2) Estimate the coordinate values of a 3D scatterer based on PSO algorithm. Take (13) as the cost function and search a 3D scatterer with the maximal value of the cost function. We denoted the estimated 3D scatterer by $\mathbf{p}_{opt} = [\hat{x}, \hat{y}, \hat{z}]^T$ and let $\Theta = \Theta \bigcup \{\mathbf{p}_{opt}\}$. The detailed procedure of PSO algorithm is discussed in [4] and [19].

Step 3) Update of the residual image. Based on the $\mathbf{p}_{opt}$ and the projection vectors $\boldsymbol{\rho}_r^k (1 \le k \le K)$ and $\boldsymbol{\rho}_a^k (1 \le k \le K)$, compute the projected scatterer positions $[i_r^k, i_a^k] (1 \le k \le K)$ where $i_r^k = \frac{\boldsymbol{\rho}_r^k \times \mathbf{p}}{\rho_r} + \frac{M_r}{2}$ and $i_a^k = \frac{\boldsymbol{\rho}_a^k \times \mathbf{p}}{\Delta f_a} + \frac{M_a}{2}$. To obtain new residual image $\mathbf{I}_k$, we set the image pixels within $\left[i_r^k - \frac{L}{2}, i_r^k + \frac{L}{2} \right]$ and $\left[i_a^k - \frac{L}{2}, i_a^k + \frac{L}{2} \right]$ to zeros, where L is a predetermined distance threshold.

Step 4) Iteration termination judgment. Compute the total image energy of the residual images, which is denoted by E_{remain}. Then calculate the ratio of E_{remain} to E_{total}. If $\frac{E_{remain}}{E_{total}} < \delta$, terminate the iteration and output Θ as the

final scatterer set. Otherwise, go back to Step 2) and continue the 3D scatterer estimation.

After the processing above, we can obtain the 3D scatterer reconstruction result of a space target.

IV. Experimental Results

In order to verify the effectiveness of the proposed method, we construct a simulated scatterer model of a satellite consisting of 24 scatterers as shown in Fig. 3. The simulated radar works in Ku band and the transmitted signal bandwidth is 1GHz. In addition, the pulse repetition frequency is 60Hz and the attitude of the simulated target remains unchanged relative to the coordinate system, which is simulated as the orbital coordinate system. The variation curves of the azimuth and pitch angles of the radar LOS in the orbital coordinate system are shown in Fig. 4 (a), which also shows that the imaging plane are not located in the same plane. Therefore, the simulation scenario can guarantee the feasibility of 3D scatterer reconstruction.

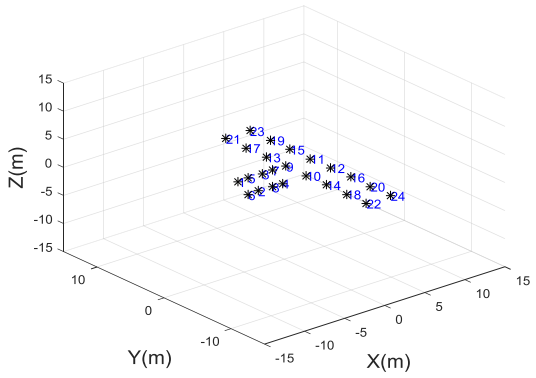

Fig. 3. Simulated scatterer model of a satellite

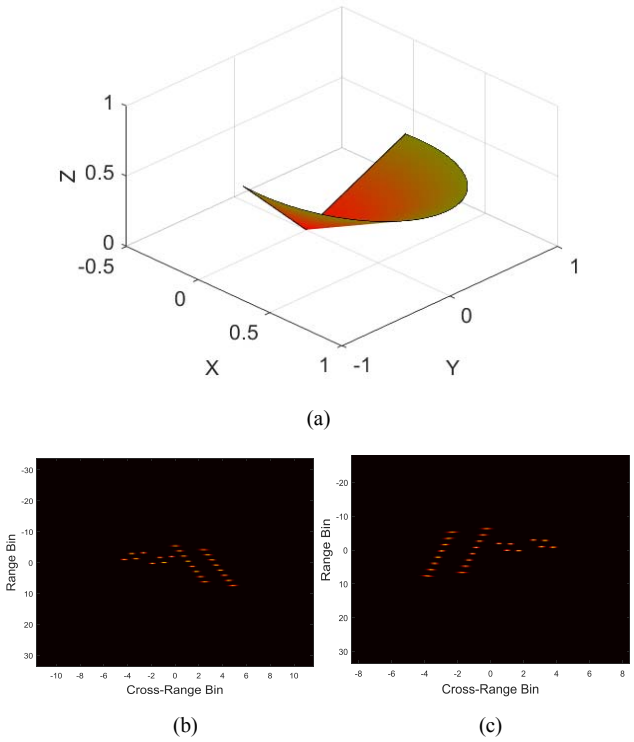

(a) (b) (c)

Fig. 4. Variation curve of the radar LOS in orbital coordinate system and partial imaging results. (a) Variation curve of the azimuth and pitch angles in orbital coordinate system. (b) 2nd ISAR image. (c) 33rd ISAR image.

In the simulation, we received 5120 echoes totally and divided them into 40 sub-apertures. The coherent processing interval of each sub-aperture is about two seconds. By performing ISAR imaging algorithm on each sub-aperture data, we can obtain the high resolution ISAR image sequence. The 2nd and the 33rd sub-aperture imaging results are shown in Fig. 4 (b) and (c), which are well focused.

According to the radar measurement information, we can construct the projection vectors corresponding to each sub-aperture. Then, the reverse projection-based 3D scatterer reconstruction method is performed on the image sequence. The 3D reconstruction result is presented in Fig. 5. Fig. 5 (a) shows the comparison between the reconstructed scatterers and the real ones while the comparisons projected on the O-XY plane, O-YZ plane and O-XZ plane are shown in Fig. 5 (b), (c) and (d), respectively.

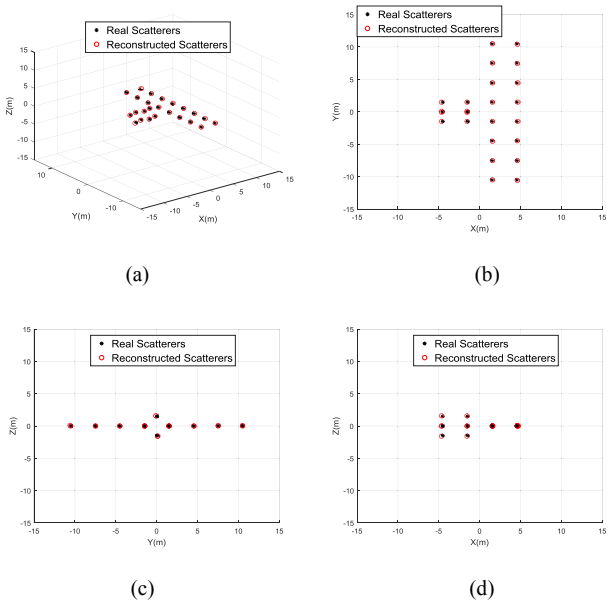

(a) (b) (c) (d)

Fig. 5. 3D reconstruction result of the simulated scatterer model. (a) Comparison between the reconstructed scatterers and the real ones. (b) The comparison result projected on the *O*-*XY* plane. (c) The comparison result projected on the *O*-*YZ* plane. (d) The comparison result projected on the *O*-*XZ* plane.

The red circles denote the reconstructed scatterers and the black asterisks represent the real ones. The comparisons illustrate that the 3D positions of each scatterer is reconstructed with high precision.

In order to evaluate the reconstruction accuracy of 3D scatterers, we introduce the root mean square error (RMSE), which is defined as

$$E_{RMSE} = \sqrt{\frac{1}{N}\sum_{n=1}^{N}\left(\mathbf{p}_{opt}^{n} - \tilde{\mathbf{p}}^{n}\right)^{2}} \tag{14}$$

where N represents the total scatterer number of the space target, $\mathbf{p}_{opt}^{n}$ denotes the reconstructed 3D coordinates of n-th scattering center, and $\tilde{\mathbf{p}}^{n}$ is the real position of n-th scattering center. Eq. (14) reflects the error between the reconstructed scatterer and the real one. The larger the E_{RMS} is, the larger the reconstruction error is, the lower the

reconstruction precision is. We can compute the RMSE is about 0.1093m, which clearly shows the high precision of the proposed method.

In addition, The 3D geometry reconstruction resolution of the proposed method can be written as

$$\Delta x \geq \max\left\{\min\left(\frac{\delta_r^1}{\left|\alpha_{11}^1\right|},\frac{\delta_f^2}{\left|\alpha_{21}^1\right|}\right),\min\left(\frac{\delta_r^2}{\left|\alpha_{11}^2\right|},\frac{\delta_f^2}{\left|\alpha_{21}^2\right|}\right),\cdots,\min\left(\frac{\delta_r^K}{\left|\alpha_{11}^K\right|},\frac{\delta_f^K}{\left|\alpha_{21}^K\right|}\right)\right\} \tag{15}$$

$$\Delta y \geq \max\left\{\min\left(\frac{\delta_r^1}{\left|\alpha_{12}^1\right|},\frac{\delta_f^1}{\left|\alpha_{22}^1\right|}\right),\min\left(\frac{\delta_r^2}{\left|\alpha_{12}^2\right|},\frac{\delta_f^2}{\left|\alpha_{22}^2\right|}\right),\cdots,\min\left(\frac{\delta_r^K}{\left|\alpha_{12}^K\right|},\frac{\delta_f^K}{\left|\alpha_{22}^K\right|}\right)\right\} \tag{16}$$

$$\Delta z \geq \max\left\{\min\left(\frac{\delta_r^1}{\left|\alpha_{13}^1\right|},\frac{\delta_f^1}{\left|\alpha_{23}^1\right|}\right),\min\left(\frac{\delta_r^2}{\left|\alpha_{13}^2\right|},\frac{\delta_f^2}{\left|\alpha_{23}^2\right|}\right),\cdots,\min\left(\frac{\delta_r^K}{\left|\alpha_{13}^K\right|},\frac{\delta_f^K}{\left|\alpha_{23}^K\right|}\right)\right\} \tag{17}$$

where δ_r^k and δ_f^k are the range resolution and cross-range Doppler resolution of k -th sub-aperture image and α_{mn}^k represents the element from m-row and n-column of the k-th sub-aperture projection vectors. And the 3D geometry reconstruction resolution of the proposed method is about $(0.2455, 0.2414, 0.2209)$.

V. Conclusion

As for the triaxial stabilized space targets, wide-angle echoes can be obtained through the long-time observation. Then high resolution 2D image sequence can be acquired. Since the attitude of the space target keeps unchanged in the orbital coordinate system, the relative motion is mainly generated by the variation of the radar LOS. Therefore, a novel 3D geometry reconstruction method is proposed by accumulating the energy of dominant scatterers in sequential ISAR images. Different with the factorization decomposition-based 3D reconstruction method, neither the scatterer extraction nor the trajectory association is the prerequisite in our method. PSO algorithm is utilized to estimate the 3D positions of the dominant scatterers one by one with simple implementation and high efficiency. Experimental results verify the effectiveness.

Acknowledgment

The authors would like to thank the anonymous reviewers for their valuable suggestions, which were of great help in improving the quality of this paper.

References

[1] F. Wang, F. Xu, Y.-Q. Jin, "Three-Dimensional Reconstruction From a Multiview Sequence of Sparse ISAR Imaging of a Space Target," *IEEE Trans. Geosci. Remote Sens.*, vol. 56, no. 2, Feb. 2018.

[2] Y. Bi, S. Wei, J. Wang and S. Mao, "3D Imaging of Rapidly Spinning Space Targets Based on a Factorization Method," *Sensors*, vol. 17, no. 2, pp. 1-18, Feb. 2017.

[3] F. Wang, T. F. Eibert, Y.-Q. Jin, "Simulation of ISAR Imaging for s Space Target and Reconstruction Under Sparse Sampling via Compressed Sensing," *IEEE Trans. Geosci. Remote Sens.*, vol. 53, no. 6, pp. 3432-3441, Jun. 2015.

[4] L. Liu, F. Zhou, M. Tao, P. Sun and Z. Zhang, "Adaptive Translational Motion Compensation Method for ISAR Imaging Under Low SNR Based on Particle Swarm Optimization," *IEEE J. Sel. Top. Appl. Obs. Remote Sens.*, vol. 8, no. 11, pp. 5146-5157, Nov. 2015.

[5] M. Martorella, F. Salvetti, and D. Stagliano, "3D Target Reconstruction by Means of 2D-ISAR Imaging and Inteferometry," in *Proc. IEEE Radar Conf. (RADAR)*, Ottawa, Canada, Apr./May 2013, pp.1-6.

[6] B. Tian, Z. Lu, Y. Liu, and X. Li, "Review on Interferometric ISAR 3D Imaging: Concept, Technology and Experiment," Signal Processing, vol. 153, pp. 164-187, 2018.

[7] F. Salvetti, M. Martorella, E. Giusti, and D. Staglianò, "Multi-View Three-Dimensional Interferometric Inverse Synthetic Aperture Radar," IEEE Transactions on Aerospace and Electronic Systems, DOI: DOI 10.1109/TAES.2018.2864469.

[8] G. Xu, M. Xing, X.-G. Xia, L. Zhang, Q. Chen, Z. Bao, "3D Geometry and Motion Estimations of Maneuvering Targets for Interferometric ISAR With Sparse Aperture," IEEE Transactions on Image Processing, vol. 25, no. 5, pp. 2005-2020, May 2016.

[9] Y. Bi, S. Wei, and J. Wang, "3D Reconstruction of High-speed Moving Targets Based on HRR Measurements," IET Radar Sonar and Navigation, vol. 11, iss. 5, pp. 778-787, May 2017.

[10] Y. Bi, S. Wei, J. Wang, Y. Zhang, Z. Sun, and C. Yuan, "New Method of Scatterers Association and 3D Reconstruction Based on Multi-Hypothesis Tracking," Journal of Beijing University of Aeronautics and Astronautics, vol. 42, no. 6, pp. 1219-1227, Jun. 2016.

[11] C. Tomasi, and T. Kanade, "Shape and Motion from Image Streams under orthography: A factorization method," Int. J. Comput. Vis., vol. 9, no. 2, pp. 137-154, Nov. 1992.

[12] T. Morita, and T. Kanade, "A sequential factorization method for recovering shape and motion from image streams," IEEE Trans. Pattern Anal. Mach. Intell., vol. 19, no. 8, pp. 858-867, Aug. 1997.

[13] J. T. Mayhan, M. L. Burrows, K. M. Cuomo, J. E. Piou, "High Resolution 3D "Snapshot" ISAR Imaging and Feature Extraction," IEEE Transactions on Aerospace and Electronic Systems, vol. 37, no. 2, pp. 630-641.

[14] F. E. McFadden, "Three-dimensional Reconstruction from ISAR Sequences," in Proc. SPIE, vol. 4744, pp. 58-67, Jul. 2002.

[15] L. Liu, F. Zhou, X.-R. Bai, M.-L. Tao, and Z.-J. Zhang, "Joint Cross-Range Scaling and 3D Geometry Reconstruction of ISAR Targets Based on Factorization Method," IEEE Trans. Image Process., vol. 25, no. 4, pp. 1740–1750, Apr. 2016.

[16] H. Ruan, Y. Wu, X. Jia, and W. Ye, "Novel ISAR Imaging Algorithm for Maneuvering Targets Based on a Modified Keystone Transform," IEEE Trans. Geosci. Remote Sens. Lett., vol. 11, no. 1, pp. 128-132, Jan. 2014.

[17] J. Zheng, H. Liu, G. Liao, T. Su, Z. Liu, and Q. H. Liu, "ISAR Imaging of Nonuniformly Rotating Targets Based on Generalized Decoupling Technique," *IEEE J. Sel. Top. Appl. Obs. Remote Sens.*, vol. 9, no. 1, pp. 520-532, Jan. 2016.

[18] Y. Wang, R. Xu, Q. Zhang, and B. Zhao, "ISAR Imaging of Maneuvering Target Based on the Quadratic Frequency Modulated Signal Model With Time-Varying Amplitude," *IEEE J. Sel. Top. Appl. Obs. Remote Sens.*, vol. 10, no. 3, pp. 1012-1024, Mar. 2017.

[19] L. Liu, M. S. Qi, F. Zhou, "A Novel Non-Uniform Rotational Motion Estimation and Compensation Method for Maneuvering Targets ISAR Imaging Utilizing Particle Swarm Optimization," IEEE Sensors J., vol. 18, no. 1, pp. 299-309, Jan. 2018.